lations (*8, 11, 12, 14, 26*) indicate that the OH distribution is a complicated function of the rates at which the rings and inner satellites produce gas, the distribution of energies imparted to newly produced molecules, and the OH molecule lifetime in the Saturn system.

REFERENCES AND NOTES

1. C. B. Pilcher, C. R. Chapman, L. A. Lebofsky, H. H. Kieffer, *Science* **167**, 1372 (1970); R. N. Clark, *Icarus* **44**, 388 (1980).
2. M. Dennefeld, in *Exploration of the Planetary Systems*, A. Woszczyk and C. Iwaniszewski, Eds. (Int. Astron. Union Symp. 65, Reidel, Dordrecht, 1974), pp. 471–472; J. Blamont, in *The Rings of Saturn* (NASA SP-343, Washington, DC, 1974), pp. 125–130. For a discussion that preceded the definitive determination of the icy composition of the rings, see H. Harrison and R. I. Schoen, *Science* **157**, 1175 (1967).
3. H. Weiser, R. C. Vitz, H. W. Moos, *Science* **197**, 755 (1977); D. L. Judge, F.-M. Wu, R. W. Carlson, *ibid.* **207**, 431 (1980).
4. A. L. Broadfoot *et al.*, *ibid.* **212**, 206 (1981).
5. See A. F. Cheng, L. J. Lanzerotti, V. Pirronello, *J. Geophys. Res.* **87**, 4567 (1982), and references therein.
6. A. J. Lazarus and R. L. McNutt Jr., *ibid.* **88**, 8831 (1983); J. D. Richardson, A. Eviatar, G. L. Siscoe, *ibid.* **91**, 8749 (1986); R. E. Johnson *et al.*, *Icarus* **77**, 311 (1989); A. Eviatar and J. D. Richardson, *Ann. Geophys.* **8**, 725 (1990); G. E. Morfill, O. Havnes, C. K. Goertz, *J. Geophys. Res.* **98**, 11285 (1993); Z. Gan-Baruch, A. Eviatar, J. D. Richardson, R. L. McNutt Jr., *ibid.* **99**, 11063 (1994).
7. T. G. Northrop and J. R. Hill, *J. Geophys. Res.* **87**, 6045 (1982); W.-H. Ip, *ibid.* **88**, 819 (1983); J. E. P. Connerney and J. H. Waite, *Nature* **312**, 136 (1984); J. E. P. Connerney, *Geophys. Res. Lett.* **13**, 773 (1986).
8. D. E. Shemansky and D. T. Hall, *J. Geophys. Res.* **97**, 4143 (1992); D. A. Hilton and D. M. Hunten, *Icarus* **73**, 248 (1988); W. H. Smyth and M. L. Marconi, *ibid.* **101**, 18 (1993); W.-H. Ip, *Astrophys. J.* **457**, 922 (1996).
9. G. E. Morfill, H. Fechtig, E. Grün, C. K. Goertz, *Icarus* **55**, 439 (1983); P. K. Haff and A. Eviatar, *ibid.* **66**, 258 (1986).
10. T. G. Northrop and J. E. P. Connerney, *ibid.* **70**, 124 (1987).
11. M. K. Pospieszalska and R. E. Johnson, *ibid.* **93**, 45 (1991).
12. W.-H. Ip, *ibid.* **115**, 295 (1995); *J. Geophys. Res.* **89**, 8843 (1984).
13. J. N. Cuzzi and R. H. Durisen, *Icarus* **84**, 467 (1990); L. Dones, *ibid.* **92**, 194 (1991).
14. D. E. Shemansky, P. Matheson, D. T. Hall, H.-Y. Hu, T. M. Tripp, *Nature* **363**, 329 (1993).
15. For a detailed discussion of the OH $A^2\Sigma^+$-$X^2\Pi$ fluorescence process and emission rates, see D. G. Schleicher and M. F. A'Hearn, *Astrophys. J.* **331**, 1058 (1988).
16. R. E. Johnson, D. E. Grosjean, S. Jurac, R. A. Baragiola, *Eos* **74**, 569 (1993); M. Shi *et al.*, *J. Geophys. Res.* **100**, 26387 (1995).
17. D. P. Hamilton and J. A. Burns, *Nature* **365**, 498 (1993); also see *Science* **264**, 550 (1994).
18. D. E. Shemansky and P. L. Matheson, in *Calibrating Hubble Space Telescope: Post Servicing Mission*, A. Koratkar and C. Leitherer, Eds. (Space Telescope Science Institute, Baltimore, MD, 1995), pp. 88–93.
19. The HST WFPC-2 team acquired images using the F300W filter during the 22 May 1995 ring-plane crossing event (HST images U2OO0101T and U2OO0103T) and the 10 August event (image U2OO0304M). Details on the scattered-light content were described in a private communication with J. T. Clarke (e-mail: clarke@sunshine.sprl.umich.edu).
20. To model the scattered light, we used a solar spectrum acquired in March 1995 by the Solar Stellar Irradiance Comparison Experiment on the Upper Atmospheric Research Satellite (*28*). The solar spectrum in the 2990 to 3200 Å region was multiplied by a factor A_λ that accounted for albedo variations in the spectrum of the source of the scattered light and for any chromatic alteration that occurred as the light was scattered within the telescope assembly. We used the polynomial form

$$A_\lambda = \sum_{k=0}^{K} a_k(\lambda - \lambda_0)^k \tag{1}$$

where λ is the wavelength, the a_k are polynomial coefficients, and λ_0 = 2990 Å. The solar spectrum was shifted in wavelength by $\Delta\lambda$ to account for shifts introduced by the gradient of scattered light across the aperture, Doppler shifts from the different velocities of Saturn and Earth at the time of the observations, and any relative FOS and SOLSTICE wavelength calibration errors. After convolving the scattered-light model with the FOS line-spread function for extended sources, $\Delta\lambda$ and a_k were determined by a least-squares analysis to find the best fit to the observed FOS spectra in two wavelength bands (2990 to 3060 and 3110 to 3200 Å) that bracket the OH $A^2\Sigma^+$-$X^2\Pi$ (0,0) emission. This procedure was performed for each target, and each model scattered-light spectrum was subtracted from the corresponding FOS spectrum. The derived A_λ curves have gradients from −9.5 to −7.5% per 100 Å in the 2990 to 3200 Å wavelength range. To estimate the magnitude of the error introduced by the scattered-light removal process, linear and quadratic forms for A_λ were used, and the differences in the residual emissions for these two cases were used as an indicator of the uncertainty of the derived OH $A^2\Sigma^+$-$X^2\Pi$ (0,0) brightness (Table 1).
21. Fluorescent OH $A^2\Sigma^+$-$X^2\Pi$ (0,0) band spectral distributions were taken from D. G. Schleicher, thesis, University of Maryland, College Park (1983).
22. The rayleigh is a unit of surface brightness equivalent to one million photons per square centimeter per second per 4π steradians. The flux received at a detector from a uniform diffuse source with brightness B in rayleighs is $F = 10^6\ B\Omega/4\pi$ (photons cm^{-2} s^{-1}), where Ω is the aperture's solid angle in steradians.
23. See J. N. Cuzzi *et al.*, in *Planetary Rings*, R. Greenberg and A. Brahic, Eds. (Univ. of Arizona Press, Tucson, AZ, 1984), pp. 73–199, and references therein.
24. Aperture-averaged brightnesses for individual target spectra were calculated by integrating model brightnesses over the 3.66–arc sec by 1.29–arc sec FOS aperture. The position angle of the long dimension of the aperture measured eastward from Saturn's north pole direction was 76.4° for targets 1, 2, and 3 and 88.0° for targets 4 and 5.
25. R. W. Carlson, *Nature* **283**, 461 (1980).
26. J. D. Richardson, *J. Geophys. Res.* **97**, 13705 (1992).
27. S. A. Budzien, M. C. Festou, P. D. Feldman, *Icarus* **107**, 164 (1994).
28. G. J. Rottman, T. N. Woods, T. P. Sparn, *J. Geophys. Res.* **98**, 10667 (1993); T. N. Woods, G. J. Rottman, G. Ucker, *ibid.*, p. 10679.

29. We would like to thank A. Roman, A. Lubenow, and the Space Telescope Moving Object Support team at the Space Telescope Science Institute for making the 1995 Saturn ring-plane crossing observations possible and J. Clarke for providing information on the scattered-light content of WFPC-2 images. Support for this work was provided by NASA through grant GO-06015.01-94A from the Space Telescope Science Institute, which is operated by the Association of Universities for Research in Astronomy under NASA contract NAS5-26555.

19 December 1995; accepted 14 March 1996

Observations of Saturn's Inner Satellites During the May 1995 Ring-Plane Crossing

Amanda S. Bosh and Andrew S. Rivkin

The 22 May 1995 Saturn ring-plane crossing was observed with the Hubble Space Telescope; the markedly reduced scattered light from the rings at this time allowed study of the small inner satellites of the Saturn system. Prometheus was further from its predicted location than expected based on uncertainties in the 1981 ephemerides propagated forward by 15 years. A body found orbiting near or within Saturn's F ring is either an F-ring shepherd or a transient clump of dust within the F ring; given its approximate brightness, the clump theory is more likely.

On 22 May 1995, the Earth passed through the plane of Saturn's rings, allowing us to view them in an edge-on configuration. During this time, the usually bright rings become faint, making this an ideal time to study the small inner satellites. These satellites have poorly defined ephemerides because they have rarely been observed. Discovered with ground-based telescopes during the 1966 and 1980 Saturn ring-plane crossings (*1, 2*) and by Voyagers 1 and 2 (*3*), these satellites include Pan, orbiting within the Encke gap; Atlas, just outside the outer edge of the A ring; Prometheus and Pandora, the F ring shepherds; Janus and Epimetheus, the coorbital satellites; Telesto and Calypso, at Tethys's L_4 and L_5 Lagrange points; and Helene, at Dione's L_4 point (*4*). Only Janus, Epimetheus, Telesto, Calypso, and Helene have been observed since 1980 (*5, 6*), leading to better determinations of libration parameters for these bodies.

For Atlas, Prometheus, Pandora, Janus, Epimetheus, Telesto, and Calypso, we examine the differences between observed and predicted locations in images of the Saturn system taken with the Wide Field–Planetary Camera 2 (WFPC2) (*7*) on the Hubble Space Telescope (HST). The Saturn system was observed on 22 May 1995 for 11 hours spanning the time of the Earth ring-plane crossing (*8*) and on 22 Novem-

A. S. Bosh, Lowell Observatory, Flagstaff, AZ 86001–4499, USA.
A. S. Rivkin, Lowell Observatory, Flagstaff, AZ 86001–4499, and Lunar and Planetary Laboratory, University of Arizona, Tucson, AZ 85721, USA.

ber 1995 for a 40-min period just after the solar ring-plane crossing. The wide-field (WF) mode was chosen over planetary-camera (PC) mode to maximize the signal-to-noise ratio of the rings at the minimum ring brightness and to include both ring ansae on the chip (*8*).

To detect faint satellites superimposed on the rings, we constructed median-subtracted frames (MSFs). We calculated the median value of each pixel from the three or four images taken in each HST orbit and then subtracted this frame from each of the composite frames to create the MSF, scaling for changing ring brightness when necessary (*8*). Thus, the MSF has none of the repeating signal sources such as ring signal, yet retains fast-moving satellites and cosmic-ray hits. To avoid missing slow-moving objects, we carefully examined the MSFs for anomalies at ansae and the raw frames for signs of any satellite predicted to be at an ansa.

All known satellites except for Pan, Atlas, and Prometheus were located within 10 pixels (1 arc sec) of their predicted positions. The three exceptions were expected to be the most difficult to find because they are close to the rings, do not have a significant known inclination, and are among the smallest and faintest of the known satellites. To locate Pan, Atlas, and Prometheus, and any new satellite candidates, we searched the MSFs using the blink technique and determined the centers for the sources (*9*). To determine the pixel location of the center of Saturn, we fitted the positions of known satellites in the images to ephemeris values for their offsets from the center of Saturn (*10, 11*). With these centers, we converted pixel locations to distances from Saturn projected onto the plane of the sky (*12*).

We first fit a circular, noninclined orbit model to the data (projected distances from Saturn versus time). The fitted parameters are orbital radius a and mean longitude λ_0 at reference time t_0 [defined to be 22 May 1995, 6:00 TDT (terrestrial dynamical time) at Saturn] with respect to the ascending node of Saturn's equator on the Earth's equator (J2000.0). We then fit an eccentric model for known satellites, fitting for a and λ_0 only, with eccentricity e and longitude of periapse ϖ_0 fixed at their known values (*5, 10, 13*). When compared against orbital parameters for the known satellites derived from other observations, the eccentric fits yield similar a values for Pandora, Epimetheus, Janus, Mimas, and Tethys but different a values for Dione, Rhea, Calypso, Telesto, and Enceladus (*14*) (Fig. 1); however, the discrepant satellites are poorly determined because the coverage within the orbit was not well distributed.

Our search for moving objects produced

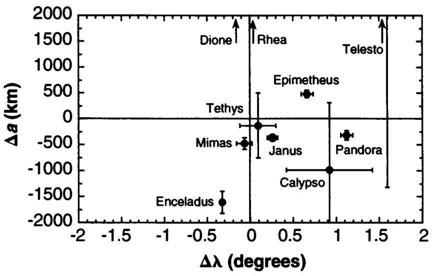

Fig. 1. Differences (observed − calculated) between fitted and previously determined values of a and λ_0 for all known satellites present in the data except for Pan, Atlas, and Prometheus.

three candidates that were tracked across multiple HST orbits (Table 1) (*15*) plus a handful of others that were visible on one HST orbit only (*16*). The three satellite candidates, 1995 S1, 1995 S2, and 1995 S3, are near the known values for Atlas, Prometheus, and the F ring, respectively. However, 1995 S1 leads Atlas's predicted longitude by 24.7° ± 0.2°, whereas the expected uncertainty in λ_0 (mean motion uncertainty propagated forward by 15 years) is of order 15°. Given that we found no other candidates of similar brightness in this region, we propose that 1995 S1 is Atlas. Corroborating evidence is provided by the observations taken on 22 November 1995, which showing a body orbiting inside the F ring on the outer edge of the A ring, leading Atlas's predicted longitude by 26.5° ± 0.6° (Fig. 2). On the basis of the May data, the revised mean motion for Atlas is 598.31282° ± 0.00005° per day. Unfortunately, Atlas was not seen clearly in data obtained either in August during the second Earth crossing or in November during the solar crossing (*17*) because of interference from other bright features. When Atlas was at ansa in August, Epimetheus was contaminating the area. There is a possible detection in three images near ansa (consistent with a location 25° ahead of the predicted λ_0) but no confirming data because of the proximity of Epimetheus. On 21 November, a bright ring arc was contam-

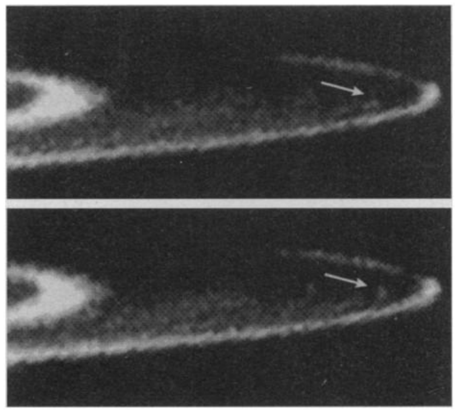

Fig. 2. Detection of Atlas (arrows) near ansa on 22 November 1995. These images of the western ring ansa were taken at 12:43 UT (top) and 12:52 UT (bottom), after the solar ring-plane crossing. At this time, we were viewing the unlit face of the rings. Images have been smoothed and contrast was enhanced to bring out faint sources; cosmic rays have been removed. In both images, the outermost bright arc is the F ring. Interior to that is the A ring, which appears dark but is dimly illuminated by sunlight reflected off of Saturn. The inner bright arc is the Cassini division.

inating the area where Atlas was expected to be.

The object 1995 S2 has the same value of a as does Prometheus, and observations in August and November 1995 (*17*) confirm that it is Prometheus. However, 1995 S2 trails the predicted λ_0 of Prometheus by almost 20°, an offset that is six to seven times greater than its predicted uncertainty. Several possibilities exist for the discrepancy: it has an unseen coorbital satellite (*17, 18*), it underwent a collision with the F ring or other body (*18*), or the magnitude of the uncertainty in its mean motion was underestimated. If Prometheus has an unseen coorbital, its λ_0 will librate over time but there would be no observable difference in λ_0 between May and November (Fig. 3). This is marginally consistent with the data if the formal errors of λ_0 are underestimates. Prometheus was expected to have collided with the F ring in February 1994 (*18*) as a

Table 1. Orbit fits to 1995 S1, 1995 S2, and 1995 S3. Eccentric orbit fits are included for 1995 S2 (Prometheus) and 1995 S3 under the assumption it is an F-ring clump. An eccentric orbit fit was not attempted for 1995 S1 (Atlas) because Atlas does not have a known eccentricity. Longitudes (J2000) λ_0 and ϖ_0 are for 22 May 1995, 6:00 TDT at Saturn.

Candidate	Fit type	a (km)	λ_0 (deg)	e	ϖ_0 (deg)	Fit rms (km)	Δa (km)	$\Delta\lambda$ (deg)
1995 S1	Circular	137,610 ± 155	57.0 ± 0.2	—	—	954	−70	24.7
1995 S2	Circular	139,545 ± 140	8.5 ± 0.2	—	—	442		
	Eccentric*	139,820 ± 160	8.3 ± 0.2	0.0024	15.07	517	440	−19.7
	Eccentric†	138,625 ± 545	9.2 ± 0.5	0.006	173	365		
1995 S3	Circular	140,830 ± 105	333.4 ± 0.1	—	—	508		
	Eccentric‡	140,460 ± 105	333.4 ± 0.1	0.0029	157.64	507	250	—

*Assumes this body is Prometheus; e and ϖ_0 held fixed at Prometheus values. †Formal error for fitted e = 0.003 and for ϖ_0 = 57. ‡Assumes this body is a clump within the F ring; e and ϖ_0 held fixed at F ring values (*17*).

result of differential apsidal precession. To create an offset as large as that observed, a collision in 1994 must have produced a change in mean motion of 0.04° per day. A change this large implies that the longitudes in May and November would differ by almost 8°, which was not observed (Fig. 3). There is significant uncertainty in the time of the F ring collision, such that it could have happened as early as 1991; this would require a change of 1° between May and August and between August and November. If we place the collision immediately after the Voyager 2 encounter instead, this implies a change of 0.33° between May and August, and 0.66° between May and November. A collision with the F ring at this epoch is not possible on the basis of the observed orientations of the orbits of Prometheus and the F ring; a collision with another body such as a comet would need to be invoked.

As a test of the stability of Prometheus's λ_0, we fit the May data including ϖ_0 and e as free parameters. This model changes the λ_0 offset by 0.9°, bringing it much closer to the observed August and November values. The actual uncertainty in λ_0 may be larger than the formal error shown by the test fit described above; this may be true for the August and November values as well. With a larger uncertainty, on the order of 1°, several of the theories for the Prometheus longitude discrepancy fall into the realm of possibility (Fig. 3): the unseen coorbital, a collision immediately after the Voyager visits, and a collision with the F ring in 1991.

The satellite candidate 1995 S3 (Fig. 4) does not have a semimajor axis near any known satellites; however, it is only 2σ from the maximum extent of the F ring and thus may be a clump of dust or an embedded satellite within the F ring. If it is not an F ring clump, then it could be a shepherding satellite of the F ring, like Prometheus and Pandora. If we assume 1995 S3 is within the F ring, we can fit an eccentric orbit model to the data, holding the values for e and ϖ_0 fixed at the values for the F ring (Table 1). The root-mean-square (rms) residual for the fit decreases slightly from that of the circular orbit fit, whereas a decreases until it is only 275 km larger than that of the ring.

To discern the true nature of 1995 S3, we need better orbital parameters and photometric information. Unfortunately, photometry on these candidates is difficult because of imperfect ring subtraction and nearby satellites; therefore, we are not able to determine brightness as a function of distance from Saturn. We can state only that 1995 S3 has about the same brightness as Atlas; therefore, 1995 S3 must be about the same size, 20 to 40 km in diameter. It is unlikely that a satellite of this size was missed during the Voyager encounters (*19*); therefore, 1995 S3 is probably an F ring clump.

Many bright clumps, both localized and elongated, were seen within the F ring during the two Voyager visits in 1980 and 1981 (*20*). These bright spots could have been dust clumps or small embedded satellites. The longer clumps disappeared rather quickly, indicating a loosely held aggregate of small particles that spreads as a result of Keplerian shear. A temporary brightening can occur if a small moonlet (large ring particle) is pulverized during a collision with another ring particle: A large cloud of small particles reflects much more light than a single particle of equivalent mass because of the increased surface area and therefore would appear bright until the particles spread uniformly around the orbit. The lifetimes of ring clumps and arcs must be shorter than the time between Voyager encounters (about 9 months) because none of the observed features could be correlated between the two visits. Here we have data taken 3 and 6 months apart that we can use to investigate the lifetimes of these clumps by searching for correspondence between 1995 S3 and other bodies observed at the August and November epochs. Of the satellite candidates observed in August and November (*17*), only 1995 S6 is a possible match: its observed longitude was ahead of 1995 S3's projected longitude by only 3° in August. Therefore, this one ring clump may have persisted for at least 3 months but not for 6 months.

We have accounted for the lost satellites Atlas and Prometheus but not for Pan. We have a tentative detection of Pan near its predicted position in three images from one HST orbit taken just after the ring-plane crossing. This body exhibits the correct projected velocity for a body within the Encke gap. We were able to determine image centers in only two images; in the third image, the body was too close to Rhea. We cannot fit an orbit with only two positions, but if we assume this is Pan, we can fix a and fit for λ_0. We find a value that leads Pan's predicted value by 5.52° ± 0.08°, implying a mean motion of 626.04510° ± 0.00004° per day. This value is similar to one Showalter found by including a tentative detection in Voyager 1 data (*1*).

These observations may be useful in answering questions about the evolution of Saturn's rings. Prometheus's orbit is expected to be evolving outward as a response to ring torques, but theory predicts it should be doing so at a much slower rate than seen here: over 10 years, the cumulative effects of ring torques would cause it to lag by 340 km, or 0.05 arc sec as seen from Earth (*21*). This lag of only 0.14° is more than two orders of magnitude smaller than the one we observed. Atlas should be evolving in the same manner, but the effect should be smaller than that for Prometheus. Although ring torques are not the answer to the mystery of why Prometheus is not nearer its predicted location, it is clear that the prob-

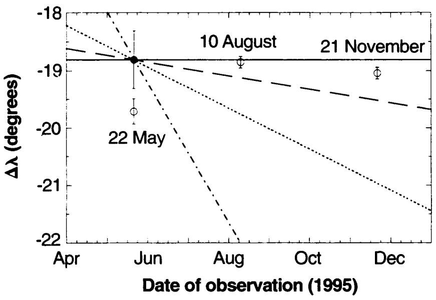

Fig. 3. Variance of Prometheus λ_0 offset. Offset values include those determined from a least-squares fit with ϖ_0 fixed at the predicted value (open circles) and another with this value and e included as free parameters (filled circle). Lines indicate the expected change in λ_0 offset with time for a collision with the F ring or another body shortly after the last Voyager 2 images of Prometheus were taken (dashed line); a collision with the F ring on 6 February 1994 as predicted by Murray and Giuliatti Winter (*18*) (dot-dashed line); a collision with the F ring in 1991, the earliest predicted in (*18*) (dotted line); and the effects of a coorbital satellite (solid line).

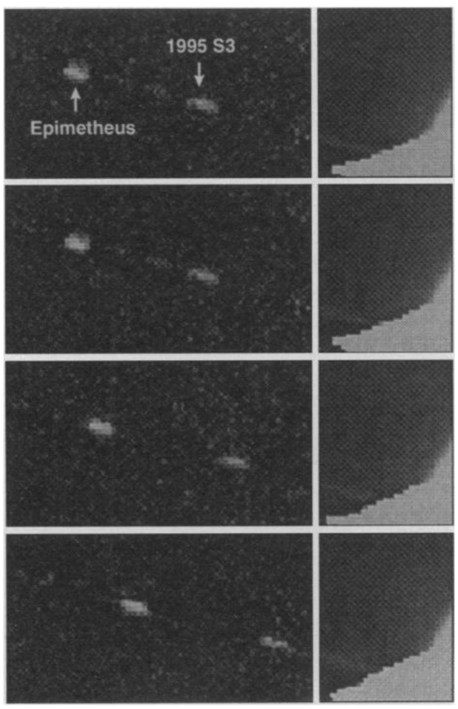

Fig. 4. Four images of 1995 S3, taken sequentially over 34 min during one HST orbit (top to bottom). Each panel is a composite of MSF (left) and raw data (right). The raw data includes part of Saturn's limb, overexposed and bleeding, and the edge-on rings, visible as a faint line just above the bleeding area. The MSF includes Epimetheus as well as 1995 S3, both moving toward Saturn.

lems with its ephemeris need to be solved if we ever hope to detect the long-term evolution of ring and satellite systems.

REFERENCES AND NOTES

1. M. R. Showalter, *Nature* **351**, 709 (1991).
2. P. Laques and J. Lecacheux, *Int. Astron. Union Circ. 3457* (1980); B. A. Smith *et al.*, *Int. Astron. Union Circ. 3466* (1980); Space Telescope Wide Field/Planetary Camera Instrument Definition Team, *Int. Astron. Union Circ. 3496* (1980); A. Dollfus, *L'Astronomie* **82**, 253 (1968); J. W. Fountain and S. M. Larson, *Icarus* **36**, 92 (1978).
3. B. A. Smith *et al.*, *Science* **212**, 163 (1981); S. P. Synnott, C. F. Peters, B. A. Smith, L. A. Morabito, *ibid.*, p. 191; B. A. Smith *et al.*, *ibid.* **215**, 504 (1982).
4. Small satellites at Lagrange points reside within stable stationary regions of the restricted three-body problem involving the satellite, Saturn, and another larger satellite (Tethys or Dione, in these cases). These satellites orbit Saturn with the same mean motion as Tethys or Dione, leading or trailing the larger satellite by 60°. The coorbital satellites Janus and Epimetheus are in a 1:1 orbital resonance. When viewed from a frame rotating with Janus, the orbit of Epimetheus resembles a horseshoe because its libration is so large (*22*).
5. P. D. Nicholson *et al.*, *Icarus* **100**, 464 (1992).
6. P. Oberti *et al.*, *Astron. Astrophys. Suppl. Ser.* **80**, 289 (1989); P. Oberti, *Astron. Astrophys.* **228**, 275 (1990); J. R. Rohde and D. Pascu, *Bull. Am. Astron. Soc.* **26**, 862 (1994).
7. C. J. Burrows, Ed., *Wide Field and Planetary Camera 2 Instrument Handbook* (Space Telescope Science Institute, Baltimore, MD, June 1995).
8. A. S. Bosh *et al.*, in preparation.
9. The three to four MSFs taken during a single HST orbit were loaded into separate image buffers, which were then displayed sequentially. Any stationary light sources remained fixed as we cycled through the buffers. With four images to blink, we could follow objects across the field, verifying true satellite-like motion. Using this technique, we searched outside the disk of Saturn to the edges of the chip (5 Saturn radii), near the plane of the rings. Centers for sources on the MSFs were determined by the centroiding routine of the IRAF software package (*23*) (for brighter satellites) or "by eye" (for fainter ones). The "by eye" method was compared with center determination on isolated satellites by IRAF centroid results on MSFs and raw frames and was found to agree to within 0.25 pixel.
10. R. A. Jacobson, *Bull. Am. Astron. Soc.* **27**, 1202 (1995).
11. Mimas and Enceladus were not used to determine the center of Saturn, even though the orbit of Mimas agreed well with its ephemeris in May. Ground-based observers reported large offsets (from predictions) in the timing of eclipses of these satellites. The only reference satellite contained in data taken in the sixth and seventh HST orbits was Mimas; an average center for Saturn for these data was computed from the remaining data and used for these images. Because of the excellent tracking of the HST, even across orbits, the location of the center of Saturn was extremely stable.
12. We accounted for field distortion across the chip using Eq. 1 of J. Holtzman *et al.*, *Publ. Astron. Soc. Pac.* **107**, 156 (1995).
13. D. Harper and D. B. Taylor, *Astron. Astrophys.* **268**, 326 (1993).
14. There is no systematic offset in *a*, indicating that there is probably no large error in the fixed value of pixel scale used. Because the WF pixel scale undersamples the point-spread function, center determination for satellite images is good to about 0.25 to 1 WF pixel (equivalent to 170 to 670 km at Saturn) for isolated satellites, more for smeared satellites or those with background contamination from other satellites or Saturn. This value is the same magnitude as the typical fit rms; therefore, differences in *a* of this order cannot be considered real.
15. A. S. Bosh and A. S. Rivkin, *Int. Astron. Union Circ. 6192* (1995).
16. An additional satellite candidate, 1995 S4, was originally reported (*15*) but was later found to depend heavily on the superposition of Telesto and this candidate at 1995 S4's elongation; although possible, this superposition is unlikely. Without the suspect data, the remaining data are not well distributed and are not sufficient to define an orbit.
17. P. D. Nicholson *et al.*, *Science* **272**, 509 (1996).
18. C. D. Murray and S. M. Giuliatti Winter, *Nature* **380**, 139 (1996).
19. S. P. Synnott, *Icarus* **67**, 189 (1986).
20. M. R. Showalter and J. A. Burns, *ibid.* **52**, 526 (1982).
21. J. J. Lissauer *et al.*, *ibid.* **64**, 425 (1985).
22. S. J. Peale, in *Satellites*, J. A. Burns and M. S. Matthews, Eds. (Univ. of Arizona Press, Tucson, 1986), pp. 159–223.
23. D. Tody, in *Instrumentation in Astronomy VI*, Tucson, AZ (SPIE 627, Bellingham, WA, 1986), pp. 733–748.

24. We acknowledge the invaluable help of A. Lubenow and A. Storrs at the Space Telescope Science Institute in scheduling these observations. We are also indebted to the HST High Speed Photometer (HSP) Instrument Definition Team, whose time was used to obtain these observations. We thank P. D. Nicholson for many enlightening discussions. A.S.B. was supported by HSP GTO grant NASG5-1613; A.S.R. was supported by NASA grant NAGW-1912. The Space Telescope Science Institute is operated by the Association of Universities for Research in Astronomy under NASA contract NAS5-26555.

4 March 1996; accepted 1 April 1996

Trapped Coronal Magnetogravity Modes

Yu-Qing Lou

Theoretical analyses suggest a physical scenario for the trapping of coronal magnetogravity wave modes above the solar transition region. The shortest oscillation period of coronal magnetogravity modes should be longer than about 1.5 hours. These long-period modes may be responsible for the unexpected low-frequency (1 to 140 microhertz) discrete modes recently discovered in interplanetary charged particle fluxes and magnetic field fluctuations. If the detected modes are caused by these magnetogravity modes rather than by gravity-mode oscillations in the solar interior, then the solar corona and the transition region may be probed from an entirely new perspective by helioseismological techniques. These coronal magnetogravity modes could reveal clues to the heating and dynamics of the solar corona.

Recently, Thomson *et al.* (*1*) reported that discrete low-frequency ($\sim$1 to 140 μHz) modes were detected in low-energy charged particle fluxes measured by Ulysses and Voyager II spacecraft by extensive time-series analysis; they also found similar modes by analyzing earlier magnetic field data from Interplanetary Monitoring Platform 8 and International Sun-Earth Explorer 3 spacecraft. Thomson *et al.* (*1*) tentatively suggested that solar interior gravity modes (*g*-modes) were propagated into the remote solar wind as fluctuations in the interplanetary magnetic field, probably as large-scale Alfvén waves (*2*), although evidence for the necessary physical linkage is apparently lacking at present. It is important to properly identify the physical and dynamic processes that lead to the appearance of these discrete low-frequency modes in order to extract useful information about the sun, its atmosphere, magnetic fields, and wind.

Theoretical models have shown that incompressible Alfvén waves decouple from compressible magnetohydrodynamic (MHD) waves in spherical geometry with a radial magnetic field (*3–6*). Gravity wave motions necessarily involve compressive effects, so it is unclear how *g*-modes trapped deep in the solar interior can be transformed into Alfvén modes propagating in the remote solar wind. Furthermore, if interior *g*-modes were transmitted into interplanetary space, their persistent passage through the photosphere should leave indelible signatures. But no evidence has been firmly established for photospheric manifestations of these interior *g*-modes (*7*). Here I offer an alternative interpretation based on a simple static atmosphere model with the appropriate wave properties to show that discrete magnetogravity modes can be trapped in the lower solar corona above the transition region and that these modes may account for the low-frequency modes detected (*1*).

The continuous expansion of the million-degree magnetized solar corona gives rise to the solar wind in interplanetary space. Close to the sun, the solar wind is sufficiently subsonic that a large coronal hole region within several solar radii can be treated as isothermal and static with a radially open magnetic field. In order to clearly explain MHD wave properties in a magnetized atmosphere and for pedagogical reasons, it would be beneficial to first consider the case without a magnetic field. An unmagnetized atmosphere can support acoustic waves when the angular perturbation frequency ω is higher than the local acoustic cutoff frequency, $\omega_c \equiv \gamma G M_\odot/(2C_s r^2)$ and gravity waves when ω is lower than the local Brunt-Väisälä buoyancy frequency, $N_{BV} \equiv (\gamma -$

Department of Astronomy and Astrophysics, University of Chicago, Chicago, IL 60637, USA.